UMERC+METS
2024 Conference

7-9 August | Duluth, MN, USA

Numerical Study on Retrievable Ocean Petal Anchor (ROPA) Behavior Supporting Marine Renewable Energy Devices

Neda Jamaleddin[a, 1], Yashar Jahanbakhsh[a], Mohammed Gabr[a], Wesley Williams[b]

[a] *North Carolina State University, Raleigh, NC, USA*
[b] *University of North Carolina at Charlotte, Charlotte, NC, USA*

Abstract

This study explores the design of an innovative anchoring foundation element, the "Retrievable Ocean Petal Anchor (ROPA)," appropriate for mooring floating Marine Renewable Energy (MRE) devices. This new and cost-effective ground anchor system is adaptable to various seabed conditions, offering flexibility in installation and retrieval. Numerical modeling within the PLAXIS 3D framework was employed to investigate how the number, deployment angle, and embedment depth of petals, along with soil properties, affect the lateral and axial capacities of ROPA in sandy seabeds. The findings show that the combined load capacity was higher in denser sand compared to looser sand and in ROPAs with larger deployment angles. Furthermore, 2-level ROPA demonstrated higher combined load capacity than 1-level ROPA across all load angles in loose sand and at load angles less than 45° in dense sand, with the maximum load capacity occurring between 45° and 60°. Additionally, higher axial-lateral load interaction was observed in ROPAs with larger deployment angles and in denser sand compared to looser sand.

Keywords: Anchoring Systems; ROPA; Marine Renewable Energy Devices

1. Introduction

Harnessing renewable energy from the ocean is garnering wide support as a promising approach for sustainable power generation. Whether self-buoyant devices such as floating wind turbines and wave energy converters or bottom-fixed devices such as wind turbines and current and tidal turbines, anchoring foundation systems supporting such devices must sustain multidirectional, time-dependent loading and vortices shedding from the mooring lines. Several anchoring foundation elements will be required, and the ability to install and retrieve these anchoring systems provides flexibility for the offshore renewable energy industry. Helical piles, or screw piles, have served as retrievable anchors since the 19th century. However, their installation in ocean environments is challenging due to the need for specialized rigs and grout to fill voids (Zhang et al., 1998). The development of ROPA addresses these challenges, providing a flexible and efficient anchoring system for offshore renewable energy devices. The ROPA concept develops a durable high-capacity anchor configuration that can be readily installed, retrieved, and reinstalled at different locations and

1 Corresponding author
E-mail address: njamale@ncsu.edu

depths. ROPA features petals that fold during installation and expand radially once deployed, enhancing anchoring efficiency. This radial expansion is facilitated by fluidizing the soil through the introduction of a high-pressure seawater jet through a truncated cone to fluidize the seabed as the petals of the anchor flare out during deployment. The flanks will expand and fold with a sliding connector ring over a central bar. Once the high-pressure stream is ended, the seabed returns to a natural state, providing resistance to pullout under loading from the marine energy device. The retrieval process is envisioned to be the inverse of the installation process. Work herein numerically examines the influence of various ROPA geometries on the lateral and axial capacities of ROPA in sandy seabeds.

2. Methodology

Numerical simulations using the PLAXIS 3D were employed to analyze the performance of ROPA under loading that leads to ultimate limit states (ULS) capacities per specifications in IEC (2006), as shown in Figure 1. The soil was modeled using the Hardening Soil (HS) model, which is well-suited for simulating the behavior of sandy soils, employing 3D 10-node tetrahedral elements. The ROPA was modeled using 6-node triangular plate elements, and its behavior was simulated using a linear elastic model. The model allowed for relative movement between the ROPA and soil using a 12-node interface element, following the method described by Brinkgreve (2014). The interface reduction factor (R_{int}) was set to 0.7, which is a typical value for pile-sand interface conditions (Jamaleddin et al., 2024). A mesh convergence study was conducted to ensure accuracy, and a fine meshing option was adopted in PLAXIS 3D.

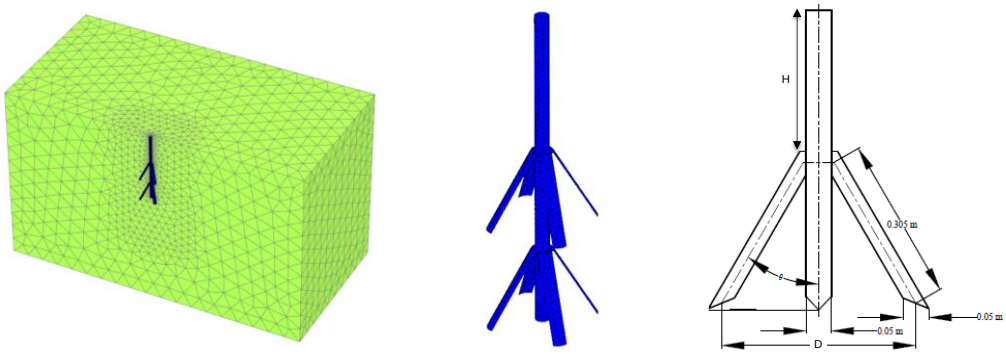

Created model in PLAXIS 3D Embedment depth ratio : H/D $D = 2 \times L \times \sin(\theta)$

Figure 1. ROPA geometry and created numerical model in PLAXIS 3D.

Soil classification and sixteen drained axial compression triaxial tests were performed to estimate the physical and shear strength properties of the sand across relative densities ranging from 20% to 70%. Samples tested at relative densities of 20% and 40% (Figure 2 (a, b)) exhibited a bulging shape after shearing, which was expected due to the relatively low-density state. The sample tested at a relative density of 53% and higher exhibited a more distinct failure plane (Figure 2 (c)). The initial tangent modulus (E_i) was determined as a function of void ratio and confining pressure by transforming the stress-strain curve into a hyperbolic form Duncan and Chang (1970). Friction angles were computed at the peak stress levels, and the results are presented in Table 1.

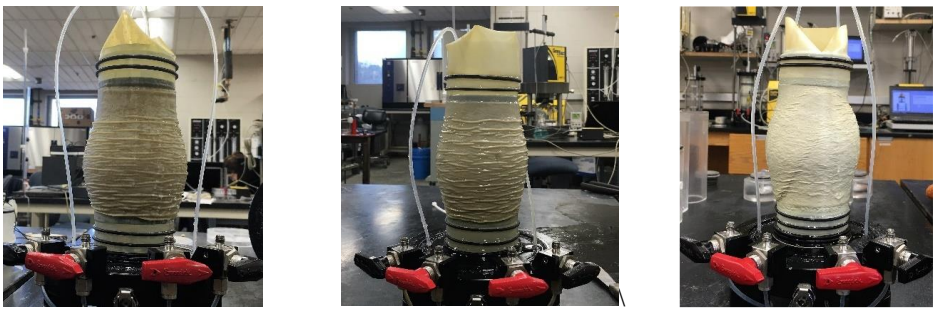

Figure 2. (a) D_R = 20%, (b) D_R = 40%, (c) D_R = 53%.

Table 1. Initial Modulus, E_i [kN/m^2], and friction angle, φ, at various relative densities

D_R (%)	E_i (kN/m^2)	ϕ (deg)
20	30,300	34.7
40	52,630	34.8
53	66,670	36.4
70	76,923	38.8

3. Results

Figure 3 presents the load-displacement curves under axial pullout load for different ROPA geometries in loose and dense sand. The results indicate a higher pullout capacity in denser sand than in looser sand and pullout capacity increasing with larger deployment angles. Interestingly, adding an additional level to the ROPA did not increase its pullout capacity, with the exception of the single-level configuration in loose sand at a deployment angle of 10 degrees. To further investigate this phenomenon, the deformation contours under axial pullout loading were examined. Deformation contours are presented in Figure 4 under axial pullout load and at 10%D for both single-level and two-level ROPA configurations with a 30-degree deployment angle, considering loose and dense sand conditions. Two failure modes, deep and shallow, were observed, depending on the embedment ratio (the embedded depth of the uppermost level over ROPA diameter, H/D) and soil properties.

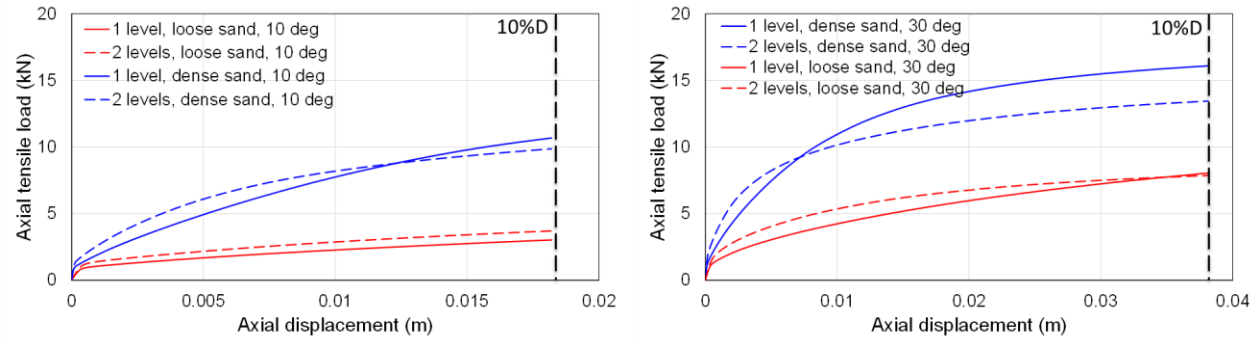

Figure 3. Load-displacement curves under axial pullout load at deployment angles of 10 deg (left) and 30 deg (right).

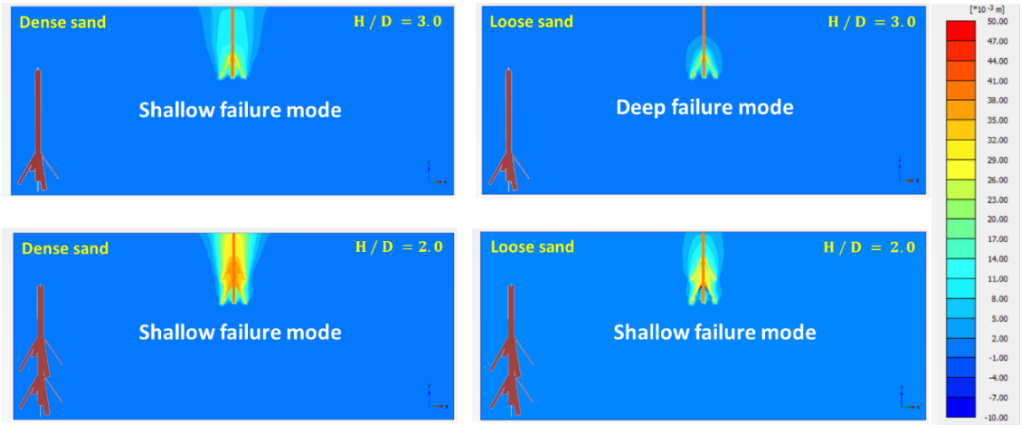

Figure 4. Deformation contours under axial pullout load and deployment angle of 30 deg.

For shallow failure mode, the bearing zone extends from the uppermost level to the ground surface. In contrast, for deep foundations, deformation contours surrounding the petals are limited below the ground surface and exhibit a

closed bulb shape. A deep failure mode for a single-level ROPA in loose sand was observed. However, by adding second petals level on top of it, the failure mode became shallow. In dense sand, the failure mode remained deep for both single-level and two-level ROPAs. Therefore, when the failure mode for a single-level ROPA is shallow, adding another level on top of it does not lead to an increase in the capacity (as the mobilized zone overlaps with that of the lower level), as the second level of petals leads to reduces the embedment ratio of the ROPA. This reduction in embedment ratio results in lower capacity as failure occurs with smaller upward displacements.

In the following, the same plots are presented for a deployment angle of 10 degrees. In dense sand, a deep failure mode was observed for single-level ROPA with an embedment depth ratio of 6, while for two-level ROPA with an embedment depth ratio of 4, the failure mode was shallow. From Figure 4 and Figure 5, it is apparent that there exists a critical embedment ratio, ranging between 2 and 3 for loose sand and between 4 and 6 for dense sand, which determines the transition from shallow to deep failure mode.

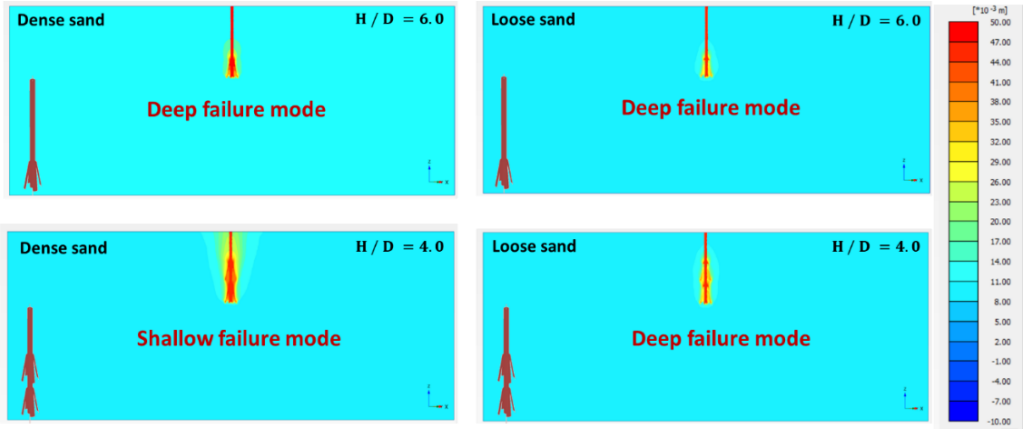

Figure 5. Deformation contours under axial pullout load and deployment angle of 10 deg.

In Figure 6, load-displacement curves under lateral loading are presented. The results indicate a higher lateral capacity in denser sand than looser sand, as well as capacity increase with the deployment angle. Moreover, a higher lateral capacity was observed in 2-level ROPA than in 1-level, due to petal contribution mobilization of larger passive soil wedge with lateral displacement.

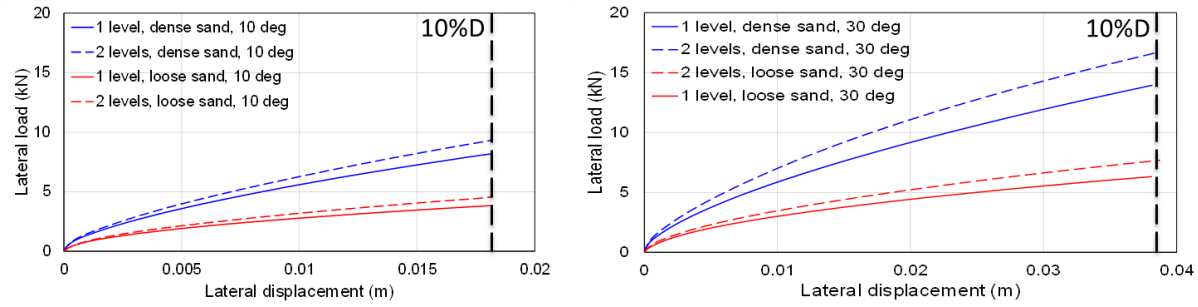

Figure 6. Load-displacement curves under lateral load at deployment angles of 10 deg (left) and 30 deg (right).

In the mooring system of floating devices, taut mooring lines and, to a lesser extent, catenary lines generate inclined forces at the anchorage foundation system. This creates both an upward vertical and a horizontal component of the load (Cerfontaine et al., 2023). The resistance that can be mobilized under combined, or 'multidirectional,' loading is characterized herein by a failure envelope known as an interaction diagram. This diagram specifies the load combinations that could result in failure, from a geotechnical design perspective. The failure envelope of ROPAs considered in our study is presented in Figure 7. As shown by the data in Figure 7, there was a higher load capacity (P) in 2-level ROPA than in 1-level in all load angles (α) in loose sand, while there was a higher load capacity in 2-level ROPA than in 1-level in $\alpha < 45°$ in dense sand. Moreover, the maximum load capacity was observed in load

angles of $45° < \alpha < 60°$ for all cases considered. To better understand the interaction between lateral and axial loadings, the top plots were normalized in terms of purely axial or lateral loading to act as normalization points (pure axial capacity = V_{max}; pure horizontal capacity = H_{max}) to study the effects of combined loading. A higher interaction, and therefore a lower normalized combined load capacity, was observed in ROPAs with a 10-degree petal deployment angle compared to those with a 30-degree angle. Moreover, there was increased interaction in dense sand compared to the loose sand. Furthermore, a higher interaction was noted in the 2-level ROPA compared to the 1-level ROPA, except for the ROPA in loose sand with a 10-degree deployment angle.

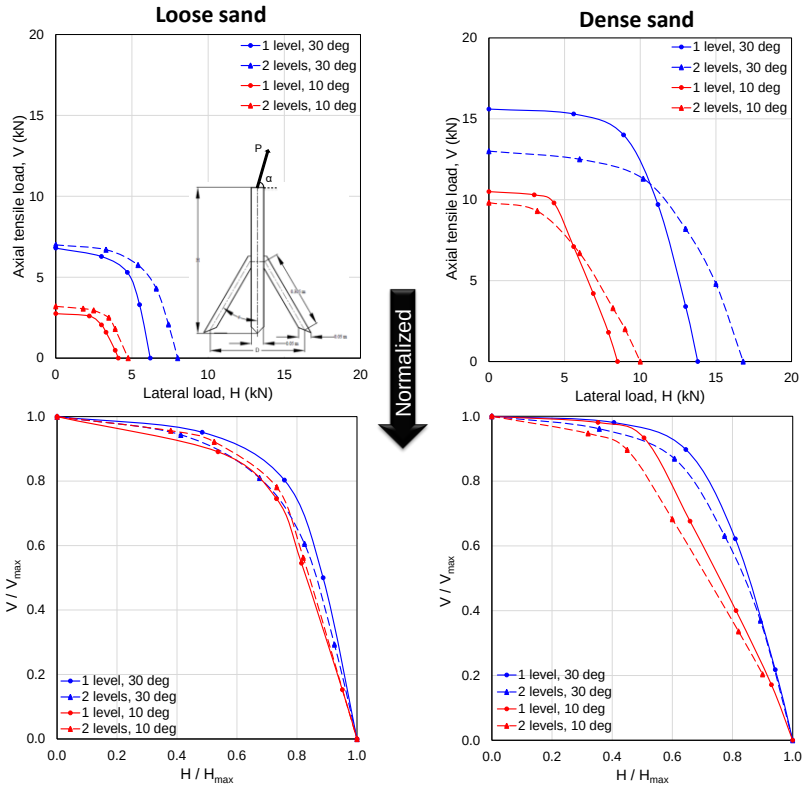

Figure 7. Failure envelope of ROPA in sand.

4. Conclusions

Numerical modeling in the PLAXIS 3D framework was employed to explore the impact of ROPA geometry and soil properties on axial and lateral capacity. Findings include:

- A higher capacity was observed in denser sand compared to looser sand, and in ROPAs with larger deployment angles.
- The axial capacity of the 2-level ROPA was only higher than that of the 1-level ROPA in loose sand with a deployment angle of 10° due to deep failure mode rather than shallow failure mode. In contrast, the lateral capacity of the 2-level ROPA exceeded that of the 1-level ROPA in all tested scenarios.
- The 2-level ROPA exhibited a higher overall load capacity than the 1-level ROPA across all load angles in loose sand and at load angles less than 45° in dense sand. The maximum load capacity was observed between load angles of 45° and 60°.
- Higher axial-lateral load interaction was noted in ROPAs with larger deployment angles and in denser sand. The 2-level ROPA generally demonstrated greater interaction than the 1-level ROPA, with the exception of instances in loose sand with a deployment angle of 10°.

Acknowledgements

This research has been supported by funding from the North Carolina Renewable Ocean Energy Program, directed by Mr. George Bonner.

References

Brinkgreve, R.B., 2014. Efficient modelling of pile foundations in the Finite Element Method. DFMEC 2014.

Cerfontaine, B., White, D., Kwa, K., Gourvenec, S., Knappett, J., Brown, M., 2023. Anchor geotechnics for floating offshore wind: Current technologies and future innovations. Ocean Engineering 279, 114327. https://doi.org/10.1016/j.oceaneng.2023.114327

Commission, I.E., others, 2006. Wind turbines-part 1: design requirements. IEC 614001 Ed. 3.

Duncan, J.M., Chang, C.-Y., 1970. Nonlinear analysis of stress and strain in soils. Journal of the soil mechanics and foundations division 96, 1629–1653.

Jamaleddin, N., Gabr, M., Borden, R., 2024. Shared Anchoring of Marine Renewable Energy Devices Utilizing Monopiles, in: Geo-Congress 2024. Presented at the Geo-Congress 2024, American Society of Civil Engineers, Vancouver, British Columbia, Canada, pp. 246–256. https://doi.org/10.1061/9780784485323.025

Zhang, D., Chalaturnyk, R., Robertson, P., Sego, D., Cyre, G., 1998. Screw anchor test program (Part I): Instrumentation, site characterization and installation, in: Proc. 51st Canadian Geotech. Conf., Edmonton. pp. 321–362.